An OGCM investigation of the Red Sea circulation. Part II.: The three-dimensional circulation in the Red Sea.

Sarantis S. Sofianos,[1]

RSMAS, University of Miami, Miami, Florida

William E. Johns

RSMAS, University of Miami, Miami, Florida

Short title: AN OGCM INVESTIGATION OF THE RED SEA CIRCULATION. PART II

Abstract.

The three-dimensional circulation of the Red Sea is studied using a set of Miami Isopycnic Coordinate Ocean Model (MICOM) simulations. The model performance is tested against the few available observations in the basin and shows generally good agreement with the main observed features of the circulation. The main findings of this analysis include an intensification of the along-axis flow toward the coasts, with a transition from western intensified boundary flow in the south to eastern intensified flow in the north, and a series of strong seasonal or permanent eddy-like features. Model experiments conducted with different forcing fields (wind-stress forcing only, surface buoyancy forcing only, or both forcings combined) showed that the circulation produced by the buoyancy forcing is stronger overall and dominates the wind-driven part of the circulation. The main circulation pattern is related to the seasonal buoyancy flux (mostly due to the evaporation) which causes the density to increase northward in the basin and produces a northward surface pressure gradient associated with the downward sloping of the sea surface. The response of the eastern boundary to the associated mean cross-basin geostrophic current depends on the stratification and β-effect. In the northern part of the basin this results in an eastward intensification of the northward surface flow associated with the presence of Kelvin waves while in the south the traditional westward intensification due to Rossby waves takes place. The most prominent gyre circulation pattern occurs in the north where a permanent cyclonic gyre is present that is involved in the formation of Red Sea Outflow Water (RSOW). Beneath the surface boundary currents are similarly intensified southward undercurrents

that carry the RSOW to the sill to flow out of the basin into the Indian Ocean.

Introduction

The Red Sea is one of the most unexplored areas of the northern hemisphere oceans. Most of the available observations are sporadic and sparse in space making any attempt to construct a picture of the three-dimensional circulation in the Red Sea very difficult. The only exception is the area of the strait of Bab el Mandeb which has attracted the interest of several observational efforts during the past century (Vercelli, 1927; Siedler, 1968; Maillard and Soliman, 1984; Murray and Johns, 1997). The circulation that emerges from these observations is a two-layer exchange flow of the inverse estuarine type that lasts from October to May, with a relatively fresh surface inflow and a deep outflow of the very saline (39.7 psu) Red Sea Outflow Water (RSOW). This simple pattern is interrupted for four months, during the summer season (June to September), when a shallow surface outflow, a subsurface intrusion of Gulf of Aden Intermediate Water (GAIW), and a weaker deep RSOW outflow take place.

North of the strait, inside the Red Sea, most of our knowledge of the circulation and distribution of oceanographic properties comes from a handful of expeditions that performed mostly hydrographic stations, and data sets from ships of opportunity which usually follow the central axis of the Red Sea. Based on this kind of data and the elongated shape of the basin most of the descriptive and theoretical investigations of the Red Sea circulation follow a two-dimensional approach (in the latitude-depth plane). Between them, the most debated aspect is the relative importance of the thermohaline

and wind forcing and their role in the circulation and stratification of the Red Sea. Because of the strong salinity gradient along the axis of the Red Sea and the formation of the very saline outflowing water mass inside the basin, the buoyancy loss (mostly due to the large evaporation rate) has been thought by several investigators as the basic controlling mechanism of the flow (Maury, 1855; Luksch, 1901; Neumann and McGill, 1962; Phillips, 1966; Tragou and Garrett, 1997). Others believe that the wind-stress field is more important in determining the circulation pattern while the thermohaline forcing plays a secondary role (Thompson, 1939a and 1939b; Siedler, 1969; Patzert, 1974a).

Very few clear circulation features can be identified from the observations performed in the Red Sea. Vercelli (1927), during a winter expedition in the southern part of the basin, measured significant northward currents close to the coasts, especially the African coast. During a later cruise (winter 1929, Vercelli, 1931) in the central Red Sea, near Port Sudan, he observed a southward countercurrent at depths greater than $250m$ in the open sea but less than $150m$ near the coast. The area where the most consistent observations were undertaken is the northern part of the basin, north of 23^o latitude. Two winter cruises (1935 on the R/V MABAHISS and 1963 on the R/V CDT ROBERT GIRAUD) acquired several hydrographic sections in the area (Morcos, 1970; Morcos and Soliman, 1974; Maillard, 1974). The patterns of the estimated geostrophic currents agree in general showing a cyclonic gyre at the extreme north which penetrates up to $300m$ depth and an anticyclonic gyre about 2 degrees to the south. The presence of the northern cyclonic eddy was later verified by a series of five drifter tracks during 1993-94

which showed a consistent cyclonic circulation north of 26^oN (Clifford et al., 1997). The temperature observations also support the presence of these features with colder waters at the center of the cyclonic flow and much warmer in the center of the anticyclonic flow. These characteristics can also be seen in later cruises (Quadfasel and Baunder, 1993) and can be attributed to vertical displacement of the isopycnals inside cyclonic and anticyclonic vortices. Thus the Red Sea appears to contain several quasi-permanent gyres and intensified boundary currents and subsurface countercurrents that are only peripherally understood.

In this study a general circulation ocean model, the Miami Isopycnic Coordinate Ocean Model (MICOM) (Bleck et al., 1992; Bleck and Chassignet, 1994), is used to investigate the three-dimensional circulation in the Red Sea. In the next section we provide background and review some existing theories on the Red Sea circulation. Next, the model configuration and the forcing fields used will be discussed. Section 4 presents the results of the numerical simulation. In Section 5 results from two additional experiments will be presented, investigating the different effects of the thermohaline and wind forcing. Finally, the last section includes a summary and discussion of the overall picture of the Red Sea circulation emerging from this study.

Background

Atmospheric Forcing

The fresh water deficit of the Red Sea is one of the largest encountered in the world ocean, due to strong evaporation, very small precipitation and negligible river runoff. The actual $E - P$ rate has been highly debated and the values proposed by different investigators range from 1.5 to 2.3 $m/year$ (Yegorov, 1950; Neumann, 1952; Privett, 1959; da Siva, et al., 1994; Tragou et al., 1999). Recent long term observations at the strait of Bab el Mandeb (Murray and Johns, 1997) of the flow and the temperature/salinity characteristics of the water masses involved can be used to constrain the average fresh water budget of the whole basin. Using this data, the annual mean $E - P$ rate is estimated at $2.06 \pm 0.22\, m/year$ (Sofianos et al., 2001). Little is known about the temporal and spatial variability of the freshwater flux and there are large discrepancies between available estimates (Yegorov, 1950; Neumann, 1952; Privett, 1959; da Siva, et al., 1994). The latent heat flux associated with the $E - P$ is very large (about 160 W/m^2), however, the net radiative heat gain nearly balances this loss, so that the annual mean heat loss from the surface of the Red Sea is small, $O(10\, W m^{-2})$, (Patzert, 1974; Tragou et al., 1999; Sofianos et al., 2001). The combined effects of freshwater and heat flux add up to an annual mean buoyancy loss of approximately $27 \times 10^{-6} kgm^{-1}s^{-3}$. According to the Comprehensive Ocean-Atmosphere Data Set (COADS) (da Silva, 1994) there is a significant seasonal cycle around this mean value with a large buoyancy loss during winter and a small buoyancy gain during summer, such that the total range of the annual cycle ($25 \times 10^{-5} kgm^{-1}s^{-3}$) is nearly equal to

the mean value. A strong south to north mean gradient in the buoyancy forcing is also present in the basin (Figure 1).

The Red Sea experiences strong and complicated wind forcing with surface winds that can reach speeds of more than $10 m/sec$, intense land and sea breezes, and synoptic time scale variability. Since the focus of this paper is on the seasonal circulation patterns, the high frequency variability will be neglected and the monthly mean wind fields will be used. Due to the existence of high mountain ranges along the African and Asian coasts, the direction of the surface winds is orographically steered along the axis of the Sea. The January and July mean fields of the wind-stress from COADS (da Silva, 1994) are plotted in Figure 2, which represent the winter and summer extremes. Two wind regimes are present, one in the northern part of the Red Sea and one in the southern part. The former is influenced by the eastern Mediterranean weather systems (Pedgley, 1974) and the wind is from the northwest all around the year. In the southern part of the basin the wind is controlled by the Indian Monsoon system and it reverses from southeast during winter (October to May) to northwest during summer (June to September). Although this general pattern has been well known for thousands of years and verified by many investigators, details of the wind field estimates differ between different data sets, especially in the northern part of the Red Sea. The Koninklijk Nederlands Meteorologisch Instituut (KNMI) atlas (1949), utilized by Patzert (1974a), shows the strongest winds during summer in the northern part of the basin while in COADS the maximum winds occur during winter. Nevertheless, the basic seasonal cycle of the wind-stress is a very robust feature and combined with the intensity of the winds

it makes the wind forcing an important mechanism for the Red Sea circulation.

Two-dimensional Circulation Models

Phillips (1966) produced a model of the circulation of the Red Sea driven by a uniform buoyancy loss from the surface of the Sea. He assumed a semi-enclosed basin with a sill at the exit and constant width. The circulation was assumed to be in steady state and two-dimensional (in the vertical plane), so that rotational effects were neglected. Based on dimensional considerations he found that the similarity solutions that can satisfy this type of model produce a two-layer convective circulation and density pattern in good qualitative agreement with several characteristics of the winter regime in the Red Sea, such as the density gradient in the south-north direction and the two-layer flow present in the strait of Bab el Mandeb. Although several problems have been identified in Phillips' model, such as the very high viscosity of the lower layer required for the solutions to match the observed exchange flow in the Red Sea (Tragou and Garrett, 1997), this approach provides a useful tool for understanding the dynamics governing semi-enclosed concentration basins. The most important disadvantage of this model is that it can represent only the winter state and gives no explanation for the intense seasonal variability observed in the southern part of the Red Sea and particularly at the strait of Bab el Mandeb. Nevertheless, it gives a strong indication of the important role of thermohaline forcing and its variability in driving the Red Sea circulation.

Another two-dimensional approach was pursued by Patzert (1974a) for explaining

the mechanisms behind the basic circulation pattern observed in the Red Sea and its exchange with the Indian Ocean. Based on the obvious coincidence of the reversal of the the wind field in the south with the reversal of the surface flow in the Bab el Mandeb strait, he hypothesized that the varying wind-stress and associated changes of the sea level in the Red Sea and the Gulf of Aden act to control the circulation. From October to May the southeasterly winds present in the southern Red Sea cause a large surface inflow which "piles-up" surface water in the central part of the Red Sea, between $16^o - 21^oN$, where the winds are convergent. North of these latitudes the winds are from the NNW and the surface flow is against the wind-stress. To explain this discrepancy Patzert proposed that a surface pressure gradient is created at the northern part of the Red Sea opposite to the wind-stress either by the large evaporation and the winter cooling in the northern end of the Sea or by the water that piles-up in the zone of convergent winds. This pressure gradient overpowers the regional wind-stress, which according to the wind data he used (KNMI) achieves its minimum during winter. To maintain continuity of mass, he assumed that the subsurface pressure gradient and the consequent flow is to the south and outside the basin toward the Gulf of Aden. This winter circulation is closed by sinking of water in the north, although Patzert did not specify the mechanisms involved in this process.

During summer, when the three-layer system is present at Bab el Mandeb, the winds are from the northwest all over the Red Sea. This is expected to induce a general surface southward flow in the Red Sea. Since the winds are rather weak in the south, Patzert assumed that another mechanism besides the direct wind-stress forcing must be

involved in generating the strong surface outflow from the Red Sea observed in summer. He proposed that outside the basin in the northwestern Gulf of Aden, wind -induced upwelling due to the favorable summer wind field takes place which lowers the sea surface elevation, producing a pressure gradient over the sill that enhances the shallow outflow from the basin. The same mechanism displaces the subsurface isopycnals upwards in the Gulf of Aden producing an opposite pressure gradient at intermediate depths capable of inducing the intermediate intrusion of GAIW. Patzert's hypothesis was the first one to describe the seasonal reversal of the surface flow and the presence of the GAIW intrusion during summer.

Although these simple two-dimensional approaches are valuable concepts of the Red Sea circulation and remain useful avenues of further research, their limitations and their inability to describe the whole picture of the basinwide circulation and stratification is obvious. For example, both theories described above predict currents of a few cm/s, but all available direct observations inside the Red Sea show that much larger velocities (up to $0.5m/s$) are possible (Vercelli, 1927; Morcos, 1970; Morcos and Soliman, 1974; Maillard, 1974). Furthermore, the cross-basin currents can be strong and appear to be related to a series of gyres and meanders all along the basin. These features may play an important role in the mixing and dissipation processes in the basin, and in some regions they may be closely linked to watermass formation processes. Therefore, to improve our understanding of the dynamics and mechanisms controlling the Red Sea circulation, the investigational approach must be extended to a three-dimensional framework.

The Model

MICOM is primitive equation ocean model that has its vertical discretization in layers of constant potential density. An advantage of isopycnic coordinates is that the vertical resolution of the model can be intensified in regions of higher gradients and the presence of different water masses can be identified clearly over the full domain used in the simulation. This is very important in the case of the Red Sea which exhibits a complex exchange flow at the strait of Bab el Mandeb and a variety of water masses involved in the general circulation of the area.

The vertical density structure is defined by 6 isopycnic layers and a variable-density mixed layer (Table 1). The choice of the number of layers and the σ_θ of each layer was made in order to incorporate all the major water masses while keeping the model simple and computationally efficient. It has been hypothesized that the core of the outflowing RSOW originates from intermediate depths in the Red Sea (Neumann and McGill, 1962; Cember, 1988; Sofianos, 2000) and so special attention was given to distinguish between deep and intermediate waters which possess similar temperature and salinity characteristics and differ only slightly in their density. The bottom layer represents the Red Sea Deep Water (RSDW) which fills the basin from about $200\,m$ to the bottom. The layers above represent the intermediate layers involved in the Red Sea circulation, and the first isopycnic layer, just below the mixed layer, represents the core of the GAIW.

The model domain includes the whole Red Sea basin and a part of the Gulf of Aden reaching to 45^{o}E (Figure 3). At the open end of the domain at 45^{o}E, a 0.5^o wide buffer zone was fitted (Figure 3) where hydrography is relaxed towards monthly mean values derived from the Levitus (1982) climatology, with a relaxation time of 60 days. In the present simulations the grid interval was chosen at 0.1^o (or about 10 km) in order to resolve the exchange flow at the narrow strait. The two gulfs at the northern end of the Red Sea (Suez and Aqaba) are very small and were not included in the experiments performed. The wind and thermodynamic forcing applied to the model are derived from COADS (da Silva et al., 1994) but with an additional 0.5 $myear^{-1}$ $E-P$ and 60 Wm^{-2} of heat loss to the atmosphere for the reasons discussed in Sofianos and Johns, 2001. The model experiments were initialized using the National Oceanographic Data Center (NODC) hydrographic data for the winter state. For more discussion of the model, its configuration, and a description of the complete series of the experiments performed, the reader is referred to Sofianos and Johns, 2001.

Three different model simulations are presented and discussed in this paper, which differ only in how they are forced. Both seasonal wind and seasonal thermohaline forcing are used for driving the model for the main experiment (E1). Two more experiments using only one of the two forcing mechanisms (thermohaline and wind) were carried out (E2 and E3, respectively). All the simulations were integrated for 10 years. Although the simulations did not reach absolute equilibrium after this time, the circulation develops very fast (within a few months) and does not change perceptively after that either in its mean or seasonal cycle. For all of the experiments the results mentioned

here are the average of the last 9 years of integration.

Results

The performance of the model was tested at the strait of Bab el Mandeb where the resulting seasonal cycle of the exchange flow was compared with the available direct observations (Sofianos and Johns, 2001). Although some differences in the phase and range of the two cycles exist, the main result is that the simulation is able to reproduce the basic characteristics of the observed variability. These features include the reversal of the surface flow in summer, the associated intermediate water intrusion, and the seasonal variability of the RSOW outflow with a minimum occurring during the summer. The strength of the annual mean exchange rate (0.38 Sv) is also nearly identical to the observed one (0.36 Sv). This increases our confidence in the results presented here, although comparison with future observations of the general circulation in the area will be a more definitive test.

Surface circulation

The 9-year average surface circulation for the winter (September to May) and summer (June to August) seasons are plotted in Figure 4 and 5, respectively. The choice of the months representing each season takes into account the seasonal patterns of the forcing fields as well as the exchange flow at the strait. Both wind and thermohaline forcing are highly variable at the seasonal time scales and thus the circulation patterns

are expected to show a strong seasonality. All the fields show a high degree of complexity with a series of eddies and jet-like currents. Although the surface layer transport averaged across the basin is relatively weak (about 0.4 Sv and decreasing slowly to the north, in agreement with the order of magnitude predicted from the two-dimensional approaches), the cross-basin transport is very strong in accord with previous observations.

South of 18^{o}N the seasonal variability is strongest as expected by the reversal of the wind field as well as the high variability of the exchange flow at Bab el Mandeb. The dominant feature in the south is a mesoscale gyre with its center located between 15^o and 16^{o}N which reverses from an anticyclonic rotation during winter to a cyclonic rotation during the summer, and achieves velocities of more than 0.5 m/s during the peak of the winter. Other features present in the area are weaker and smaller and most of them have a transient character.

During winter, a strong surface inflow occurs at the strait. After entering the basin this NNW flow intensifies along the western boundary as a strong boundary current with maximum velocities that vary with the strength of the inflow but are greater than 20cm/s throughout the season. After flowing only about 400 km into the Red Sea, near 16^{o}N, this current ceases and an eastward intensified boundary current is observed for most of the remaining length of the basin. Although this boundary current is a little weaker and more variable than its southern counterpart, and it interacts with other features of the circulation (mesoscale cyclonic and anticyclonic eddies), it accounts for most of the surface northward flow in the basin.

During summer the northward western boundary current disappears in the southern part of the Red Sea. It is during this season when the surface flow reverses and a strong intermediate inflow of the fresher and colder GAIW takes place. The model circulation now is relatively weaker and more irregular than in winter, since both wind and thermohaline forcing are weaker in summer.

In the northern part of the Red Sea, two permanent eddies dominate the circulation field, a small anticyclonic gyre centered around 23.5^oN and a larger, more elongated cyclonic gyre centered around 25^oN. Both coincide surprisingly well with available observations in the region (Morcos, 1970; Morcos and Soliman, 1974; Maillard, 1974; Clifford et al., 1997). Although their strength, shape and extent show some seasonal variability, they are present throughout the year. The stronger one is the cyclonic gyre in the north reaching maximum velocities of more than $40\,cm/s$. This particular features will be discussed in further detail later in the paper in association with intermediate water formation.

The annual mean surface temperature and salinity fields are plotted in Figure 6. There is a distinct salinity gradient toward the north where it reaches its maximum, in agreement with the observations and simple theoretical models. The temperature pattern is more complicated, presenting its maximum at the center of the basin and decreasing towards the two ends of the Red Sea. This is related to the very weak wind speed observed in the central region of the Red Sea where the wind field is convergent for most of the year. These simple pictures are altered by the circulation complexity, and areas of minima and maxima are associated with the dominant features of the circulation

pattern. A better idea of the temperature and salinity distribution and their association with the circulation and the atmospheric forcing is shown by the seasonal distribution of the two fields presented in Figure 7(a-d). During summer the surface temperatures become very warm over the whole basin and therefore the annual mean pattern, with its maximum at mid-basin, is mostly set by the winter pattern. However, it is very interesting to note the seasonal variability of zonal temperature gradient. During winter the highest temperatures are located at the eastern boundary (especially in the southern and central Red Sea), while during summer the eastern boundary is characterized by much lower temperatures (especially the northern and central Red Sea). This difference is associated with the prevailing winds which induce coastal upwelling along the eastern boundary in summer and downwelling in winter in the southern part of the basin. This effect is also reflected in the seasonal salinity distribution, where fresher surface waters are found along the eastern boundary in summer associated with upwelling of the cooler and fresher GAIW that is advected into the basin at this time of year.

Figure 8 presents the 9-year average of the annual mean sea surface elevation anomaly. Apart from the highs and lows related to the circulation pattern, there is a downward tilt of the sea level to the north. Since the freshwater flux is imposed as a "virtual salinity flux" at the mixed layer, it can not affect the volume of the basin. Thus the tilt is associated with the steric effect caused by the strong north-south density gradient through the basin.

The annual mean surface circulation and surface density are plotted in Figure 9 and will be compared with the results from two additional experiments described in

following sections. Although this is an average of the 9 years of simulation, including both seasons, some of the most important features are present, such as the boundary currents, the anticyclonic eddy in the south and the double gyre system in the northern part of the basin. This happens because some of the features are permanent and also because the winter season lasts about three fourths of the year and presents a more vigorous circulation than the summer one.

Intermediate circulation

The most active subsurface layer is the second one from the bottom (layer 6), which overlies the RSDW layer that contains a very weak circulation. Layer 6 is the core of the RSOW where most of the hypersaline outflow (39.8 psu from the model results compared to 39.7 psu from observations (Murray and Johns, 1997)) takes place at the bottom of the strait of Bab el Mandeb. The winter and summer circulation in this layer are plotted in Figure 10 and 11. The velocity field is weaker than the surface but involves several interesting features. It is also much less seasonally variable than the surface layer. The overall flow is southward and its magnitude increases to the south near the Bab el Mandeb due to topographic constrictions and because of entrainment from the adjacent layers. It is obvious that the main surface circulation features directly affect the flow at this intermediate level, such as the the strong gyres in the north which extend to the depth of layer 6. Boundary intensification is also observed in this layer, especially south of 20^oN. The general pattern of this intensification has the characteristics of an undercurrent (i.e., opposite to the surface boundary currents) but the transition point

is shifted to the north and the currents are affected by topography. Reaching the strait, the velocities in this layer become very large, achieving values of over $0.5\,m/s$.

It should be noted that the magnitude of the intermediate depth circulation in summer may be overestimated by the model because the outflow of RSOW in the model, while smaller in summer, does not decrease to the very low values seen in observations (see Sofianos and Johns, 2001). One would therefore expect the intermediate undercurrents to be considerably weaker in summer, since they are the primary conduits for transporting the RSOW water to the southern Red Sea and the Bab el Mandeb strait. The overall seasonality of the intermediate depth circulation may thus be larger than predicted by the model.

Formation of the Red Sea Outflow Water

The location, time and mechanisms involved in the formation of the RSOW inside the Red Sea basin are not yet clear. Until recently the outflowing water mass was confused with the RSDW. Most investigators agree that the RSDW is formed during winter in the Gulf of Suez (Maillard, 1974; Wyrtki, 1974) where that water obtains extreme values of salinity and sinks to the bottom of the Red Sea basin entraining ambient water. The Gulf of Aqaba is thought to be a secondary source of RSDW (Wyrtki, 1974). Other modes of formation have been hypothesized, such as open ocean deep convection and formation on the continental shelf of the Red Sea, but there is no evidence to support them. The idea that the outflow originates from intermediate

depths was proposed by Neumann and McGill (1962). Analyzing tracer distributions (^{14}C and ^{3}He) from the GEOSECS Indian Ocean Expedition, Cember (1988) was the first to clearly identify a different water mass comprising the core of the outflow (which he called RSOW to distinguish it from the RSDW). Further evidence in support of this hypothesis is the small rate of RSDW formation. The only direct observation of the transport at the mouth of the Gulf of Suez during the winter is that of Maillard (1974) during 1971-72 which gives an estimated deep water outflow of $0.082\,Sv$, or, assuming that this is representative of three winter months, an annual rate of approximately $0.02\,Sv$. Maillard (1974) assumed that this transport is doubled due to entrainment, so that the total RSDW production is $O(0.04\,Sv)$. This is a very small amount compared to the total outflow from the Red Sea which is an order of magnitude larger. Recent observations in the Red Sea (Woelk and Quadfasel, 1996) of the oxygen distribution verify the distinction between the deep and intermediate waters. An oxygen minimum at intermediate depths (about $300\,m$) separates a relatively new intermediate water mass (the RSOW) from much older deep water (RSDW).

Cember (1988) proposed that this intermediate water mass is injected immediately beneath the pycnocline at a rate of $0.11 \pm 0.02\,Sv$, and located the place of formation at the extreme open northern Red Sea. Unfortunately, no direct observations are available to verify this hypothesis, and due to insufficient data very little can be said about the mechanisms involved in this formation process.

Since the strength and properties of the exchange flow at Bab el Mandeb are well reproduced by the model (Sofianos and Johns, 2001), its results may be used to

investigate mechanisms involved in the RSOW formation, possible locations, and rates of production. The most likely area for RSOW formation is the northern Red Sea, since the strongest buoyancy forcing takes place there (Figure 1). Localized open ocean deep and intermediate convection is one of the most important mechanisms of water mass formation in the oceans and is present in many polar or low-latitude semi-enclosed basins such as the western Mediterranean (Swallow and Caston, 1973; Leaman and Schott, 1991) the eastern Mediterranean (Lascaratos, 1993), the Labrador Sea (Clarke and Cascard, 1983), the Greenland Sea (Schott et al., 1993; Visbeck et al., 1995) and Weddell Sea (Gordon, 1978; Muench, 1988; Alverson and Owens, 1996). Although localized buoyancy loss can be important in these features, the typical atmospheric scale of forcing is an order of magnitude larger than the observed structures. Furthermore, vertical stratification and the Coriolis force act together against convective motions. In order for deep or intermediate convection to take place two more conditions must also contribute, weak stratification and a "trapping mechanism" to keep the surface waters exposed to strong atmospheric forcing for enough time to acquire the proper temperature and salinity characteristics. These elements are known as the preconditioning phase (Swallow and Caston, 1973; Hogg, 1973) which can result from a variety of mechanisms. In most of the known cases this preconditioning is associated with a cyclonic gyre where the stratification weakens due to upward tilt of the isopycnals and waters are exposed for a considerable time to intense buoyancy loss. In the eastern Mediterranean, where the atmospheric conditions resemble those of the northern Red Sea (i.e., extensive evaporation), the formation of the Levantine Intermediate Water is a localized winter

process in the region of the Rhodes Gyre in the Levantine basin (Lascaratos et al., 1993). The depth in which the convective plumes penetrate depends on the vertical stratification and the time and intensity of the buoyancy flux.

The results of the model simulation suggest that a similar process is involved in the RSOW formation in the northern Red Sea. In Figure 12 the density and velocity of the surface layer is plotted for different months representing the "preconditioning" and actual formation periods. As noted before, the most significant circulation feature is the permanent cyclonic gyre centered at about 25^oN. Inside this gyre the mixed layer achieves high densities throughout the year and at the peak of the winter season the mixed layer has density close to the RSOW layer. The "trapping ability" of this gyre is also evident from the density patterns. The mixed layer density and underlying layer thicknesses along a transect through the northern Red Sea for November, February, and April, averaged over the last 9 years of simulation, are presented in Figure 13. These months coincide with the "preconditioning" phase, the period when the strongest intermediate water formation takes place, and the period when the mixed layer retreats due to buoyancy addition from the surface fluxes. The higher densities near 25^oN (Figure 13a) is clear evidence of weaker stratification inside the gyre, enabling a more efficient homogenization of the upper water column. During February (Figure 13b) the mixed layer is very deep (reaching 300 m depth at the northern end of the basin) and penetrates up to the sixth layer (the layer which corresponds to the core of the RSOW). The sixth layer disappears north of about 24^oN. This is the actual formation period, when the RSOW is replenished through open ocean convection. Following the formation

phase, the mixed layer retreats quickly and the stratification is reestablished, as shown in the April transect (Figure 13c). The sixth layer reinflates progressively filled with the newly formed RSOW.

In order to get a more quantitative estimation of the amount of RSOW produced in the area of the cyclonic gyre, the mean overturning circulation on a σ_θ-latitude plane is plotted in Figure 14. Since this is an average over all the months and the nine years of simulation it is a smooth representation of the mass fluxes inside the basin. The lowest latitude that the southern edge of the cyclonic gyre reaches during the year is 23.5^oN. The total formation of RSOW north of this latitude is about 0.25 Sv or about 65% of the RSOW outflow. The remainder is formed north of 20^oN latitude. Thus it can be concluded that the dominant formation region for the RSOW is the northern Red Sea where the cyclonic gyre and strong buoyancy forcing in winter provide a favorable environment for intermediate depth convection.

Thermohaline- and wind-driven experiments

Although the effects of the wind stress and the thermohaline forcing do not add linearly to drive the general circulation, it is sometimes convenient to separate them and investigate the circulation produced by each one (what is usually called the wind- and thermohaline-driven parts of the circulation). Mechanistically these forcings interact through the effect of wind speed on the air-sea buoyancy fluxes and stirring the mixed layer, and dynamically they interact to produce the final circulation and

stratification patterns. With the above caveats in mind, two experiments with the same configuration, described in Section 3, were carried out (E2 and E3) but with one forcing field "turned off", wind and thermohaline respectively. The main goals of these additional experiments are twofold: to estimate the relative strength and importance of each mechanism in the general circulation and, if possible, to determine the role each one plays in driving the key features of the circulation pattern presented in the previous section.

The annual mean surface velocity fields for the thermohaline- and the wind-driven cases are plotted in Figures 15 and 16, respectively. It is obvious from a comparison between the two results that the purely wind-driven circulation is much weaker than the thermohaline-driven one. This is not a result of the annual averaging, but persists throughout the year. Another indication that the thermohaline forcing is the dominant forcing mechanism is that in the areas where these two mechanisms compete with each other the patterns generated by the thermohaline forcing are the ones that prevail. This is the case in the northern end of the Red Sea, where the wind-driven circulation is anticyclonic while the thermohaline forcing drives a strong cyclonic eddy, which is a permanent feature of the circulation in the area as shown in the previous section and verified by observations. In areas where the two results have similar features (as in the case of of the winter anticyclonic eddy around 16^oN), they reinforce each other producing stronger circulation patterns. In a very few locations there are features of the circulation that appear to be specifically linked to the winds, for example, the western boundary flow that is present in the combined forcing experiment near 22^oN is present

only in the wind driven experiment. However, it is clear that the general circulation pattern of the combined forcing experiment mostly follows that of the thermohaline forced experiment.

Boundary current structure and intensification

It is very interesting to notice that the thermohaline-driven result presents a similar type of intensification towards the coasts as seen in the combined forcing experiment (E1), with boundary currents shifting from the west to east coasts at midbasin, though shifted to the north by a few degrees relative to E1. This vigorous and complicated pattern of the thermohaline circulation is in sharp contrast to previous studies (Phillips, 1966; Tragou and Garrett, 1997) that predict a sluggish and two-dimensional type of circulation. Theoretical investigation can help give some insight into the possible mechanisms involved in these patterns. A relevant study is that by McCreary et al. (1986), who investigated the effect of thermohaline forcing on the set-up of eastern boundary currents. If the density increases poleward, as is the case in the Red Sea, the resulting surface elevation field slopes downward in the same direction creating an eastward geostrophic current in the basin. This will affect the eastern boundary where downwelling must take place. McCreary et al. incorporated this idea to a three-dimensional, linear, continuous stratified theoretical model and solved for both steady forcing and forcing that oscillates in time with frequency σ. For the inviscid case, the solution at the eastern boundary will involve waves that are described by the dispersion relation

$$k = -\frac{\beta}{2\sigma}\left[1 - \left(1 - 4\frac{\sigma^2\alpha^2}{\beta^2}\right)^{1/2}\right] \quad (1)$$

where k is the zonal wavenumber, σ is the forcing frequency, $\alpha_\eta^{-1} = 2\,\Omega\,sin(\theta)/c_\eta$ is the Rossby radius of deformation of the η^{th} normal mode (with speed c_η) and $\beta = 2\,\Omega\,cos(\theta)/R$ is the meridional change of the Coriolis parameter, where R is the earth's radius. The radicand vanishes at a latitude, the critical latitude θ_{cr}, given by

$$\theta_{cr} = tan^{-1}(c_\eta/2R\sigma) \quad (2)$$

North of θ_{cr}, k is complex representing Kelvin waves that decay offshore rapidly with an e-folding scale of the order of α^{-1}. South of the critical latitude, k is real and the waves that are generated are Rossby waves that propagate offshore (westward). So, we expect a westward intensification of the meridional flow south of θ_{cr} as Rossby waves propagate the pressure gradient to the western boundary, and eastward intensification north of θ_{cr}, as indicated in the schematic of Figure 17.

Direct application of the above formulas to the model results is difficult, since the stratification and the thermohaline forcing vary in space and time and cannot be compared with the idealized functions used in the theoretical model. Nevertheless, using the annual frequency and the basinwide mean stratification from the thermohaline-driven experiment results, the critical latitude is estimated at about 17^{o}N (for the second baroclinic mode which is dominant in the Red Sea circulation, presenting a two-layer flow on the top of a mostly inactive layer). The addition of the wind does not significantly

change the circulation pattern but is able to change the stratification enough to shift the critical latitude to the south. Using the mean stratification from the main experiment (with both forcing fields) the new critical latitude is estimated at about 14.5^oN, which is consistent with the southward shift of the boundary current transition in the experiment E1 compared to the thermohaline-only experiment (E2). While it is pointless to press the details of this comparison, these results strongly suggest that the meridional surface density gradient in the Red Sea is the main factor responsible for the transition of the boundary current system from the western to the eastern boundary at midbasin. This switch of the boundary current system is an interesting and robust feature of the circulation pattern in the model that awaits verification by observations.

Summary and Discussion

The numerical simulation study of the Red Sea presented here suggests several interesting features of the circulation in the area. The most important findings include the intensification of the flow toward the coasts, the presence of the permanent double gyre system in the northern part of the basin, and the stronger seasonality of the flow in the southern part of the basin. A particularly interesting finding is the transition from western to eastern intensified boundary current regions between the southern and northern parts of the basin predicted by the model. As more observations become available and modelling efforts become more sophisticated, ideas about the circulation in the Red Sea are changing rapidly. The picture of a sluggish circulation proposed

by the simplified two-dimensional approaches seems inadequate to describe the Red Sea dynamics. The patterns of the circulation are vigorous and complicated. These differences will have an important effect on the mixing processes and may answer some puzzling questions concerning the large-scale dynamical balances and net dissipation rates in the basin (Tragou and Garrett, 1997; Sofianos, 2000).

Overall the thermohaline forcing seems to be the most important mechanism driving this highly complex circulation. The main circulation pattern is related to the buoyancy loss (mostly due to evaporation) which increases the density to the north and produces a northward pressure gradient associated with the sloping of the sea surface. An eastward mean cross-basin geostrophic current is established in the upper layer. The response of the eastern boundary depends on the stratification and β-effect, and two different regimes were identified. North of a critical latitude an eastward intensification is expected and south of it the more traditional westward intensification by Rossby waves takes place. Undercurrents are evident in the model results, but show a northward shift and some phase differences with respect to the surface currents which can be associated with the interaction of these intermediate currents with the bottom topography.

Although less important, the effects of the wind field are also evident in the results, especially at the southern part of the Red Sea where the winds have their greatest variability and become very strong during winter. The winds in the southern Red Sea affect strongly the exchange flow at the strait of Bab el Mandeb and through this the dynamical balances of the whole basin.

Future observations and numerical simulations can hopefully produce a more accurate and complete picture of the Red Sea circulation. The weakest point of all the attempts is our understanding of the air-sea fluxes in the area. Although recent observations enable us to put some constraints on the fluxes, our knowledge of the spatial and temporal variability of the forcing fields is very poor. The use of real fresh water fluxes rather than a virtual salt flux is another important improvement for future modelling attempts. The addition or subtraction of fresh water from the surface of the sea may play a role in the general dynamics of the area, and give rise to additional Goldsbrough-Stommel type circulation elements (Goldsbrough, 1933; Stommel, 1957 and 1984).

The only direct observations of the circulation in the area of the RSOW formation shown by the model come from a series of drifter tracks (Clifford et al., 1997) during different seasons and years. All drifter tracks show a cyclonic rotation and, although the number is small (5), they support favorably the results presented here. So, the scenario proposed in this paper is that a large proportion (about 65%) of the hypersaline outflow exiting the strait of Bab el Mandeb is produced in a cyclonic gyre at the northern end of the Red Sea. This is twice the rate of RSOW formation proposed by Cember (1988). It is important to note that the results presented here are from a model which is forced by climatological (monthly mean) conditions of the Red Sea. In most of the explored cases of open ocean deep or intermediate water formation, the associated processes are taking place on shorter times scales, during events of especially strong atmospheric forcing (Leaman and Schott, 1991). The investigation of the effect of the variability of

the atmospheric forcing at frequencies higher than the seasonal (synoptic time scales) is very important for our understanding of this kind of process. Thus, a logical next step is to perform numerical experiments including synoptic atmospheric forcing.

More observations are needed in the Red Sea to determine the spatial structure and seasonality of the general circulation and to test the results of model simulations. Apart from a few known features (e.g., the cyclonic gyre in the north) and the well-documented exchange at Bab el Mandeb, many features of the circulation remain obscure. Especially near the boundaries there are few observations and these will be essential to determine whether the boundary currents and gyres predicted by these simulations exist.

Acknowledgments. This work is supported by Office of Naval Research contract N00014-95-1-0025.

References

Alverson, K., and W. B. Owens, 1996, Topographic preconditioning of open-ocean deep convection, *J. Phys. Oceanogr.*, 26, 2196-2213.

Bleck, R., C. Rooth, D. Hu, and L. T. Smith, 1992, Salinity-driven thermocline transients in wind- and thermohaline-forced isopycnic coordinate model of the North Atlantic, *J. Phys. Oceanogr., 22,* 1486-1505.

Bleck, R., and E. P. Chassignet, 1994, Simulating the oceanic circulation with isopycnic-coordinate models, in: *The Oceans: Physical-chemical dynamics and human impact*, S. K. Majumar, E. W. Miller, G. S. Forbes, R. F. Schmalz, and A. A. Panah eds., The Pennsylvania Academy of Science, Pennsylvania, 17-39.

Bryden, H. L., and H. M. Stommel, 1984, Limiting processes that determine basic features of the circulation in the Mediterranean Sea, *Oceanol. Acta, 7,* 289-296.

Cember, R. P., 1988, On the sources, formation, and circulation of Red Sea Deep Water, *J. Geophys. Res., 93,* 8175-8191.

Clarke, R. A., and J. C. Gascard, 1983, The formation of Labrador Sea Water, Part I: Large-scale processes, *J. Phys. Oceanogr.*, 13, 1764-1778.

Clifford, M., C. Horton, J. Schmitz and L. H. Kantha, 1997, An oceanographic nowcast/forecast system for the Red Sea, *J. Geophys. Res., 102,* 25101-25122.

da Silva, A. M., C. C. Young, and S. Levitus, 1994, Atlas of surface marine data 1994. Volume 1: Algorithms and procedures. *NOAA Atlas NESDIS 8,* U. S. Department of Commerce, NOAA, NESDIS, 83 pp.

Goldsbrough, G., 1933, Ocean currents produced by evaporation and precipitation, *Proc. Roy. Soc. London, A141,* 512-517.

Gordon, A. L., 1978, Deep Antarctic convection west of Maud Rise, *J. Phys. Oceanogr.*, 8, 600-612.

Hogg, N. G., 1973, The prconditioning phase of Medoc 1969 - II. Topographic effects, *Deep-Sea Res.*, 20, 449-459.

Koninklijk Nederlands Meteorologisch Instituut, 1949, Red Sea and Gulf of Aden oceangraphic and meteorological data, *Publication 129,* 26 pp.

Kraus, E. B., and J. S. Turner, 1967, A one-dimensional model of the seasonal thermocline. II. The general theory and its consequences, *Tellus, 19,* 98-105.

Lascaratos, A., 1993, Estimation of deep and intermediate water mass formation rates in the Mediterranean Sea, *Deep-sea Res.*, 40, 1327-1332.

Lascaratos, A., R. G. Williams, and E. Tragou,1993, A mixed-layer study of the formation of Levantine Intermediate Water, *J. Geophys. Res.*, 98, 14739-14749.

Leaman, K. D., and F. A. Schott, 1991, Hydrographic structure of the convection regime in the Gulf of Lions: Winter 1987, *J. Phys. Oceanogr.*, 21, 575-598.

Luksch, 1901, Expedition S. M. POLA in das Rota Meer, nordliche Halfte (October 1895 - Mai 1896). Wissenschaftliche Ergebnisse, physikalische Untersuchungen, *Denkschrift d. kaiserl. Akad. Wissensch. in Wien, 69,* 337pp.

Maillard, C., 1974, Eaux intermediaires et formation d'eau profonde en Mer Rouge, in: *L'oceanographie physique de la Mer Rouge*, CNEXO, Paris, 105- 133.

Maillard, C., and G. Soliman, 1984, Hydrography of the Red Sea and exchanges with the Indian Ocean in summer, *Oceanol. Acta, 9,* 249-269.

Maury, M. F., 1855, *The physical geography of the sea and its meteorology,* The Harvard Library, Cambridge, Mass, 432 pp.

McCreary, J. P., S. R. Shetye, and P. K. Kundu, 1986, Thermohaline forcing of eastern boundary currents: With application to the circulation off the west coast of Australia, *J. Mar. Res., 44,* 71-92.

Morcos, S. A., 1970, Physical and chemical oceanography of the Red Sea, *Oceanogr. Mar. Biol. Ann. Rev., 8,* 73-202.

Morcos, S., and G. F. Soliman, 1974, Circulation and deep water formation in the Northern Red Sea in winter (based on R/V Mabahiss sections, January- February, 1935), in: *L'oceanographie physique de la Mer Rouge*, CNEXO, Paris, 91-103.

Muench, R. D., 1988, Relict convective features in the Weddell Sea, in: *Deep Convection and Deep water Formation in the Oceans*, P. C. Chu and J. C. Gascard, Eds., Elsevier, 53-67.

Murray, S. P., and W. Johns, 1997, Direct observations of seasonal exchange through the Bab el Mandeb strait, *Geophys. Res. Let., 24,* 2557-2560.

Neumann, J., 1952, Evaporation from the Red Sea, *Israel Explor. J., 2,* 153-162.

Neumann, A. C., and D. A. McGill, 1962, Circulation of the Red Sea in early summer, *Deep-Sea Res., 8,* 223-235.

Patzert, W. C., 1974a, Wind-induced reversal in Red Sea circulation, *Deep-Sea Res., 21,* 109-121.

Patzert, W. C., 1974b, Volume and heat transports between the Red Sea and Gulf of Aden, notes on the Red Sea heat budget, in: *L'oceanographie physique de la Mer Rouge*, CNEXO, Paris, 191-201.

Phillips, O. M., 1966, On turbulent convection currents and the circulation of the Red Sea, *Deep-Sea Res., 13,* 1149-1160.

Privett, D. W., 1959, Monthly charts of evaporation from the Indian Ocean (including the Red Sea and the Persian Gulf), *Q. Jl. R. Met. Soc., 85,* 424-428.

Quadfasel, D., and H. Baunder, 1993, Gyre-scale circulation cells in the Red Sea, *Oceanol. Acta, 16,* 221-229.

Schott, F., M. Visbeck, and J. Fischer, 1993, Observations of vertical currents and convection in the central Greenland Sea during the winter of 1988-89, *J. Geophys. Res.*, 98, 14401-14421.

Siedler, G., 1968, Schichtungs- und Bewegungsverhaltnisse am Sudausgang des Roten Meeres, *"Meteor" Forschungsergebn, A(4),* 1-76.

Siedler, G., 1969, General circulation of the water masses in the Red Sea, in: *Hot brines and recent heavy metal deposits in the Red Sea*, E. T. Degens and D. A. Ross eds., New York, 131-137.

Sofianos, S. S., 2000, Circulation and water mass formation in the Red Sea, and the exchange with the Indian Ocean, PhD Thesis, University of Miami.

Sofianos, S. S., W. E. Johns, and S. P. Murray, 2001, Heat and freshwater budgets in the Red Sea from direct observations at Bab el Mandeb, Deep-Sea Res., (Submitted).

Sofianos, S. S., and W. E. Johns, 2001, An OGCM investigation of the Red Sea circulation. Part II.: The exchange between the Red Sea and the Indian Ocean, (Submitted).

Stommel, H.,1957, A survey of ocean current theory, *Deep-Sea Res., 4,* 149-184.

Stommel, H.,1984 The delicate interplay between wind-stress and buoyancy nput in ocean circulation: the Goldsbrough variations, *Tellus, 36,* 111-119.

Swallow, J. C., and G. F. Caston, 1973, The preconditioning phase of MEDOC 1969 - I. Observations, *Deep-Sea Res.*, 20, 429-448.

Thompson, E. F., 1939a, Chemical and physical investigations. The general hydrography of the Red Sea, *John Murray Expedition 1933-34, Scienific Reports, 2,* 83.

Thompson, E. F., 1939b, Chemical and physical investigations. The exchange of water between the Red Sea and the Gulf of Aden over the "Sill", *John Murray Expedition 1933-34, Scienific Reports, 2,* 105.

Tragou, E., and C. Garrett, 1997, The shallow thermohaline circulation of the Red Sea, *Deep-Sea Res., 44,* 1355-1376.

Tragou, E., C. Garrett, R. Outerbridge, and G. Gilman, 1999, The heat and freshwater budgets of the Red Sea, *J. Phys. Oceanogr., 29,* 2504-2522.

Vercelli, E., 1927, Richerche di oceanografia fisica eseguite della R. N. AMMIRAGLIO MAGNAGHI (1923-24), Part IV. La temperatura e la salinita, *Annali Idrografici, 11,* 1-66.

Vercelli, E., 1931, Nuove richerche sulli correnti marine nel Mar Rosso, *Annali Idrografici, 12,* 1-74.

Visbeck, M., J. Fischer, and F, Schott, 1995, Preconditioning the Greenland Sea for deep convection: Ice formation and ice drift, *J. Geophys. Res.*, 100, 18489-18502.

Woelk, S., and D. Quadfasel, 1996, Renewal of deep water in the Red Sea during 1982-1987, *J. Geophys. Res.*, 101, 18155-18165.

Wyrtki, K., 1974, On the deep circulation of the Red Sea, in: *L'oceanographie physique de la Mer Rouge*, CNEXO, Paris, 135-163.

Yegorov, N. I., 1950, Calculation of the heat balance of the Red Sea, *Meteorologia igidrologia, 3,* 49-56.

S. Sofianos, Department of Physics, University of Athens, University Campus Build. PHYS-5, Athens 15784, Greece (e-mail:sofianos@oc.phys.uoa.gr)

W. E. Johns, Rosenstiel School of Marine and Atmospheric Science, University of Miami, 4600 Rikenbacker Causeway, Miami FL 33149, USA (e-mail:wjohns@rsmas.miami.edu)

Received _____

[1]Now at Department of Physics, University of Athens, Athens, Greece

Figure 1. Annual mean distribution of the buoyancy flux over the Red Sea, using the COADS climatology (adjusted to recent heat and freshwater fluxes estimates (Sofianos et al., 2001)).

Figure 2. Wind-stress fields for (a) January and (b) July from COADS climatology.

Figure 3. The domain and its bathymetry included in the OGCM experiments.The area indicated by red color is the location of the buffer zone where hydrography is relaxed to Levitus climatology.

Figure 4. Mean winter surface circulation from MICOM simulation, using all forcing fields (experiment E1). The result represents the last 9 years of simulation.

Figure 5. Mean summer surface circulation from MICOM simulation, using all forcing fields (experiment E1). The result represents the last 9 years of simulation.

Figure 6. Annual mean sea surface temperature (a) and salinity (b) from MICOM simulation (experiment E1 - average over the last 9 years of simulation).

Figure 7. Seasonal sea surface temperature and salinity distribution. In the upper panel the (a) winter (November-March) and (b) summer (June-September) sea surface temperature is plotted, while in the lower panel the (c) winter and (d) summer sea surface salinity (experiment E1 - average over the last 9 years of simulation).

Figure 8. Annual mean sea surface elevation anomaly from MICOM simulation (experiment E1 - average over the last 9 years of simulation).

Figure 9. Annual mean surface circulation superimposed on the mixed layer density from the full-forcing MICOM simulation (9-year average).

Figure 10. Mean winter layer 6 circulation from MICOM simulation, using all the forcing fields (experiment E1).The result represents the last 9 years of simulation.

Figure 11. Mean summer layer 6 circulation from MICOM simulation,using all the forcing fields (experiment E1).The result represents the last 9 years of simulation.

Figure 12. Mean surface velocity and density from the MICOM simulation at the northern Red Sea for (a) November and (b) February. In the lower panel (c) the location of the vertical section presented in Figure 13 is indicated by the red line.

Figure 13. Vertical stratification along a section following the central axis of the northern Red Sea for (a) November, (b) February, and (c) April, representing the sequence of "preconditioning", formation, and retreat of the mixed layer phases, respectively.

Figure 14. Mean overturning circulation from the MICOM simulation. The thick vertical line shows the southernmost annual limit of the northern cyclonic gyre where most of the RSOW is formed.

Figure 15. 9-year average sea surface velocity from the MICOM experiment driven by the thermohaline fields only (E2).

Figure 16. 9-year average sea surface velocity from the MICOM experiment driven by the wind-stress fields only (E3).

Figure 17. Schematic presentation of the flow intensification toward the coasts.

Table 1. Vertical resolution (layer density) used in the model.

LAYER NUMBER	LAYER DENSITY (kgm^{-3})	DESCRIPTION
1	mixed layer	surface layer
2	1025.75	core of the GAIW
3	1026.25	
4	1026.75	
5	1027.25	
6	1028.00	core of the RSOW
7	1028.60	RSDW

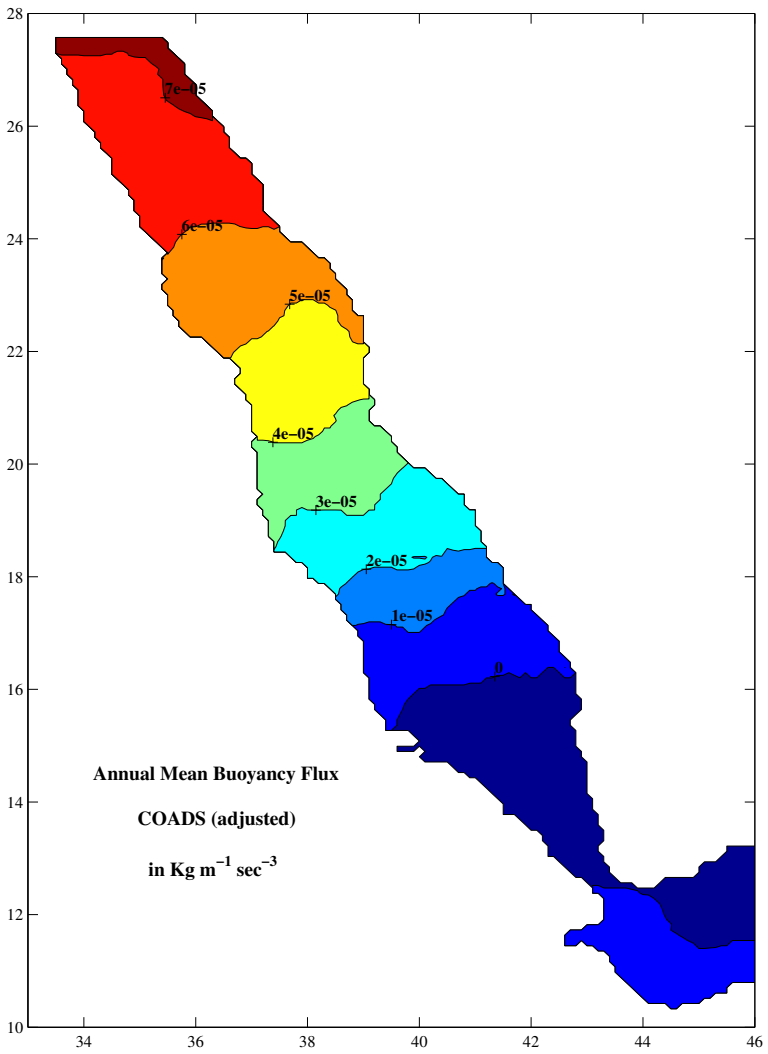
7e−05
6e−05
5e−05
4e−05
3e−05
2e−05
1e−05
0
Annual Mean Buoyancy Flux
COADS (adjusted)
in Kg m^{-1} sec^{-3}
28
26
24
22
20
18
16
14
12
10
34
36
38
40
42
44
46

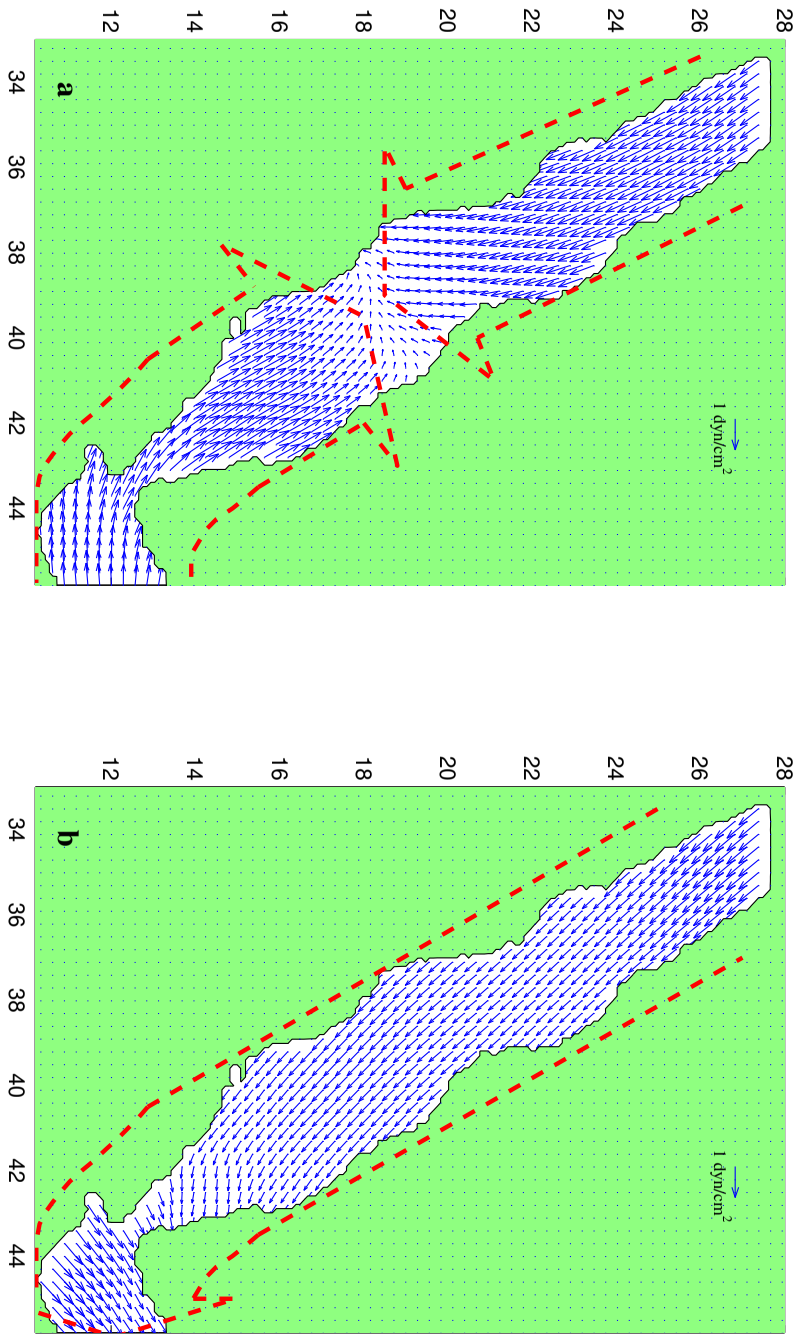
a
b
12
14
16
18
20
22
24
26
28
34
36
38
40
42
44
1 dyn/cm^2

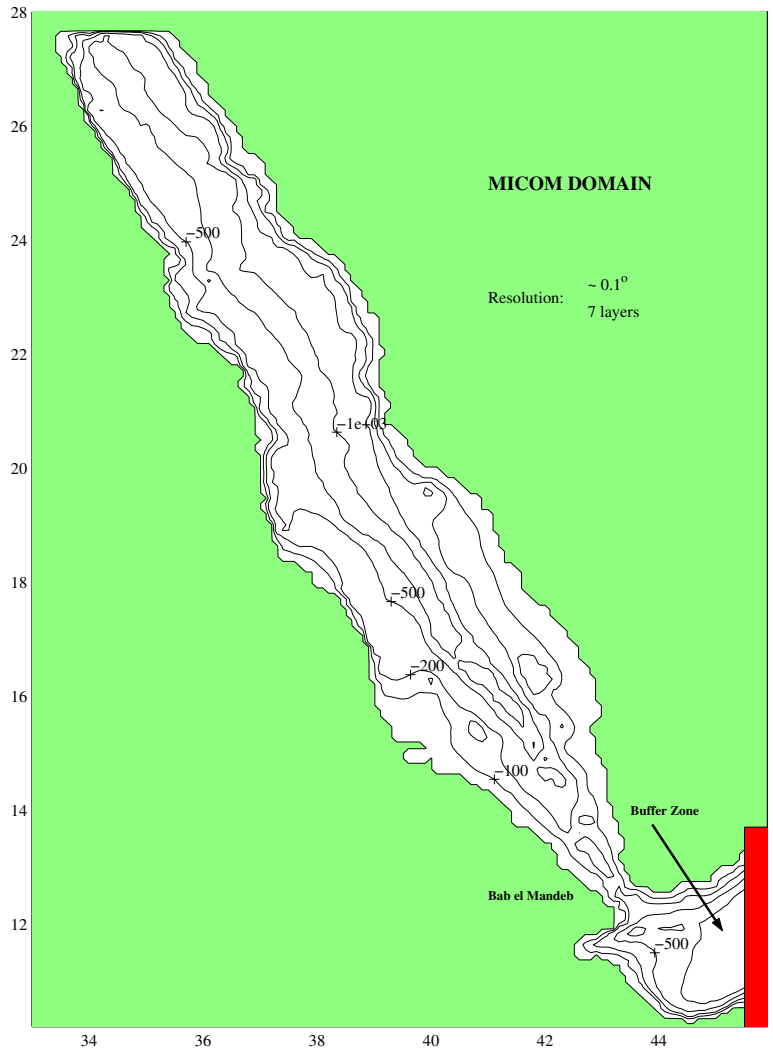
MICOM DOMAIN
Resolution: ~ 0.1°
7 layers
-500
-1e+03
-500
-200
-100
-500
Buffer Zone
Bab el Mandeb
28
26
24
22
20
18
16
14
12
34
36
38
40
42
44

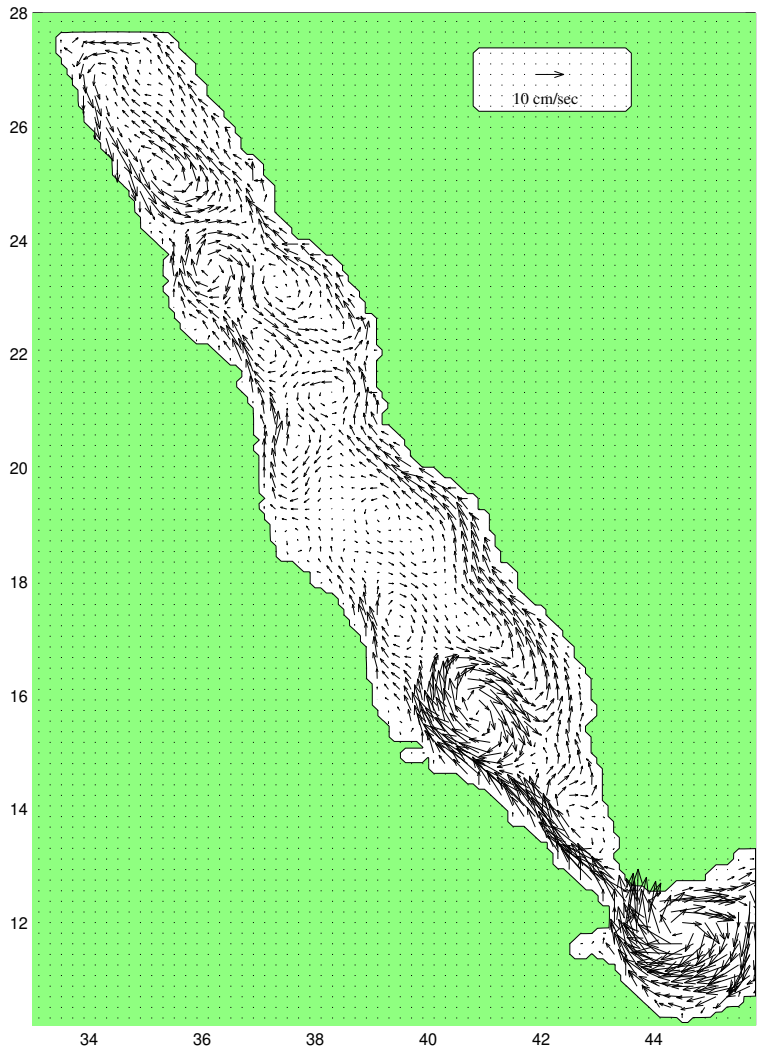
10 cm/sec
28
26
24
22
20
18
16
14
12
34
36
38
40
42
44

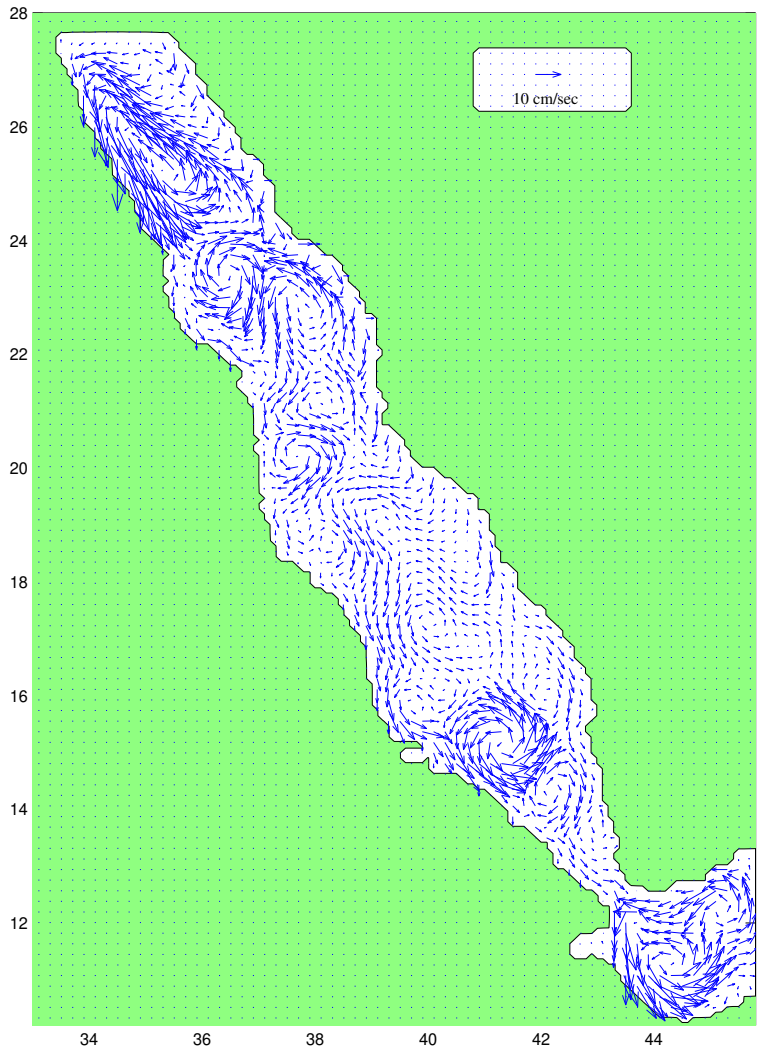
10 cm/sec
28
26
24
22
20
18
16
14
12
34
36
38
40
42
44

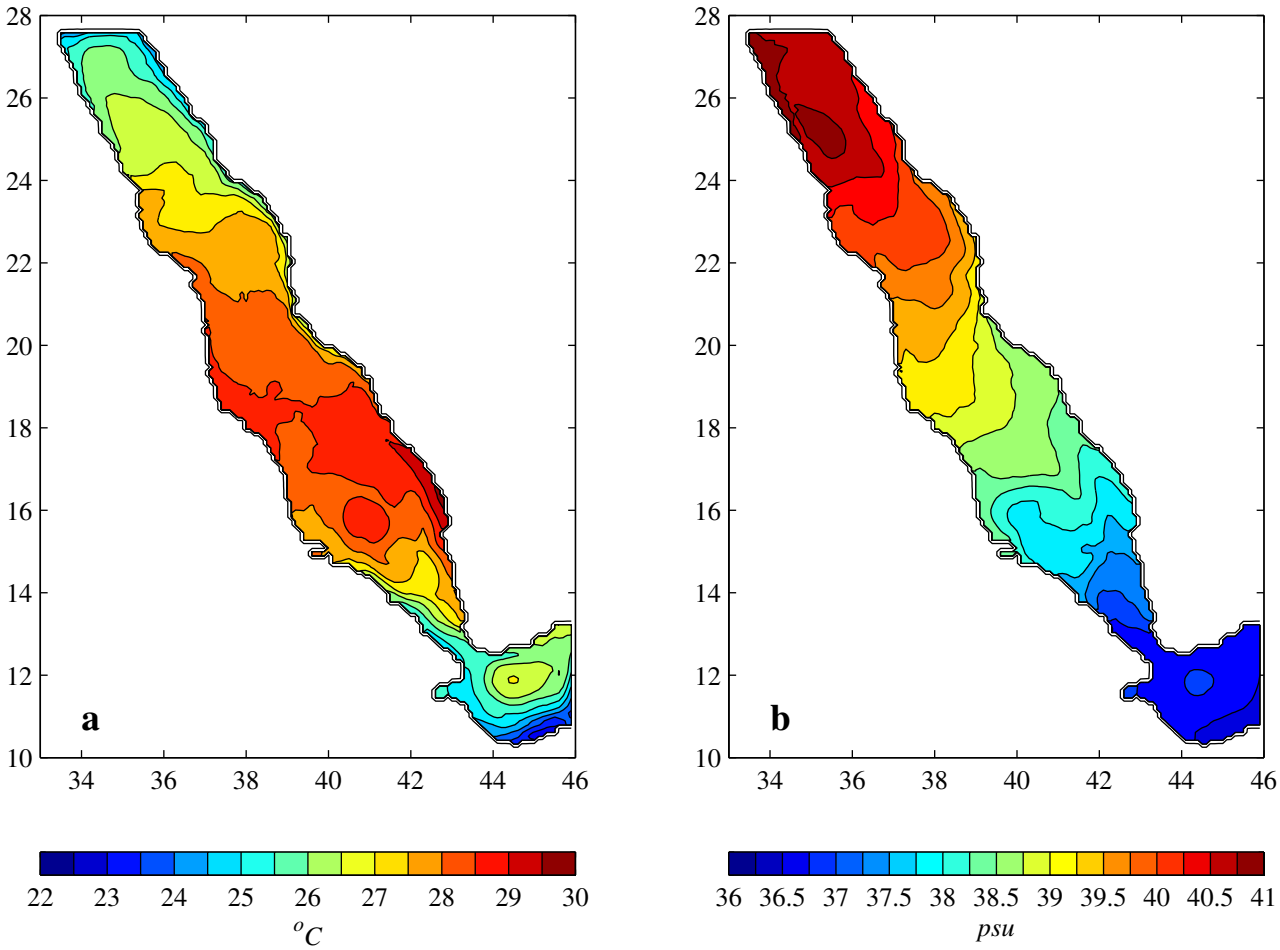
28
26
24
22
20
18
16
14
12
10
34
36
38
40
42
44
46
a
22 23 24 25 26 27 28 29 30
°C
b
36 36.5 37 37.5 38 38.5 39 39.5 40 40.5 41
psu

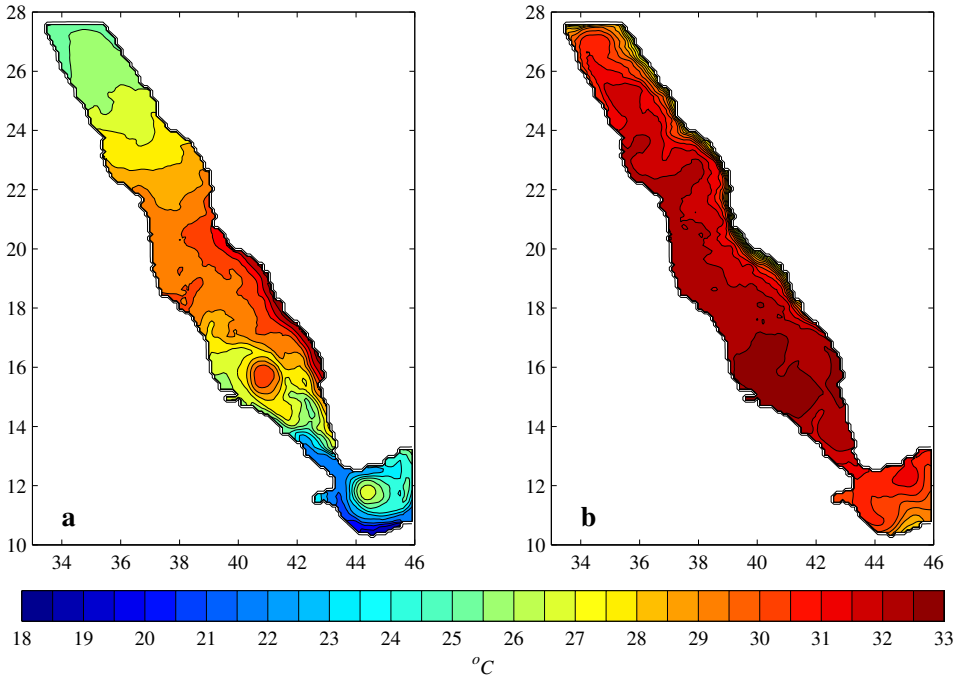
a
b
c
d
28
26
24
22
20
18
16
14
12
10
34
36
38
40
42
44
46
18
19
20
21
22
23
24
25
26
27
28
29
30
31
32
33
°C
36
36.5
37
37.5
38
38.5
39
39.5
40
40.5
41
psu

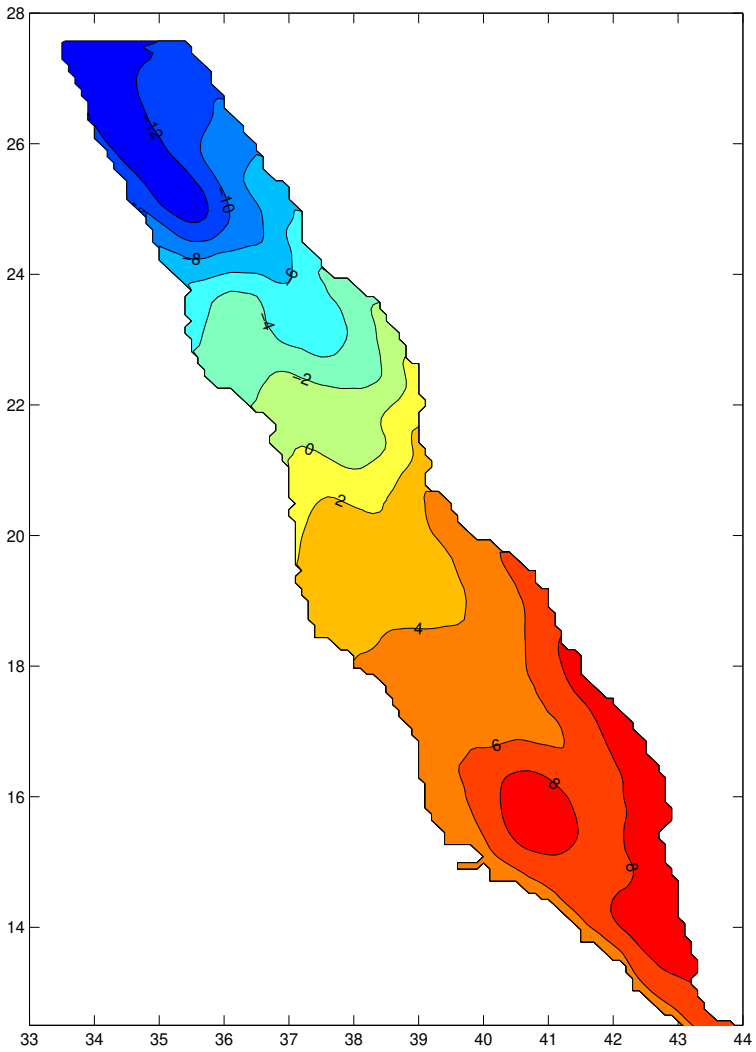
28
26
24
22
20
18
16
14
33
34
35
36
37
38
39
40
41
42
43
44
-12
-10
-8
-6
-4
-2
0
2
4
6
8
8

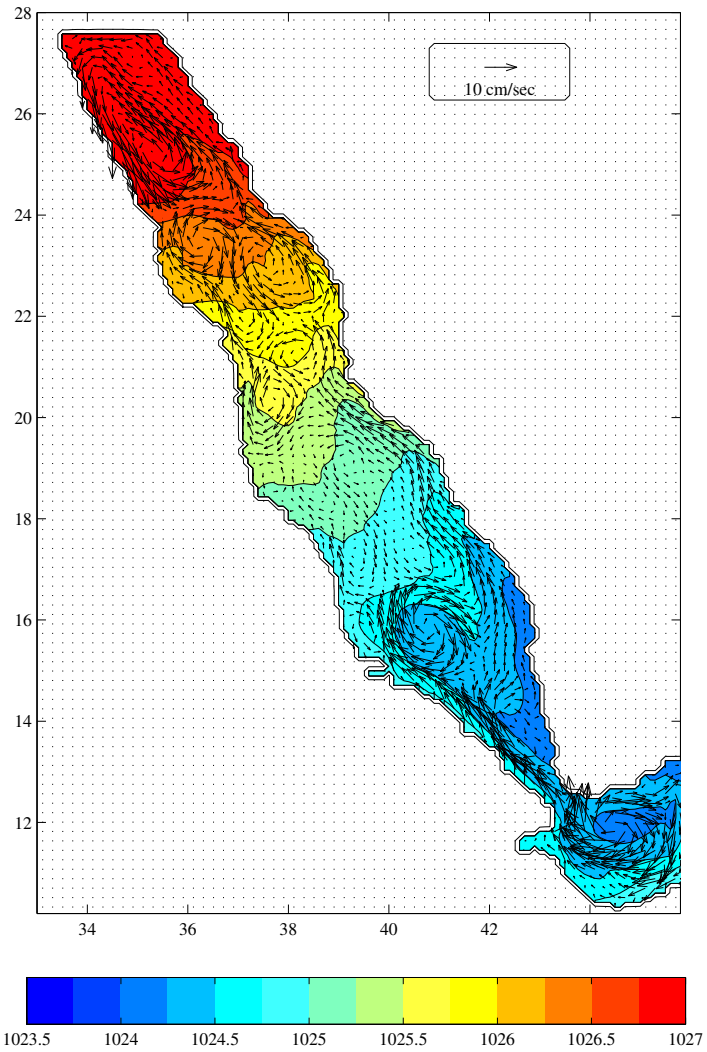
10 cm/sec
28
26
24
22
20
18
16
14
12
34
36
38
40
42
44
1023.5
1024
1024.5
1025
1025.5
1026
1026.5
1027

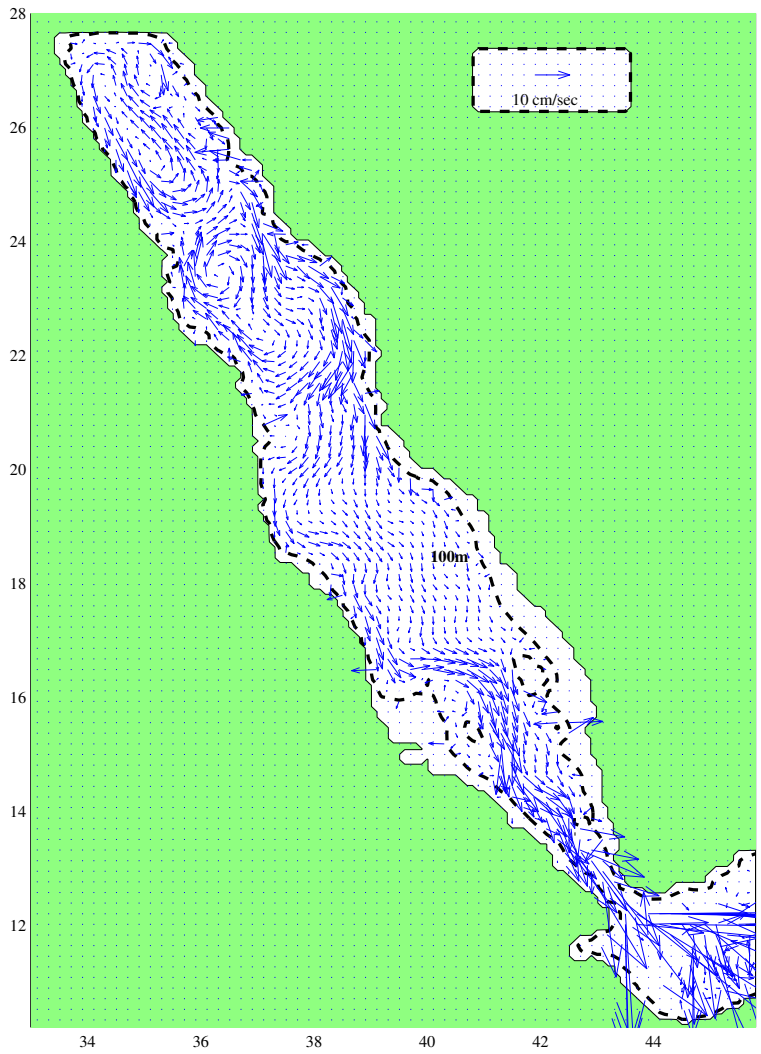
10 cm/sec
100m
28
26
24
22
20
18
16
14
12
34
36
38
40
42
44

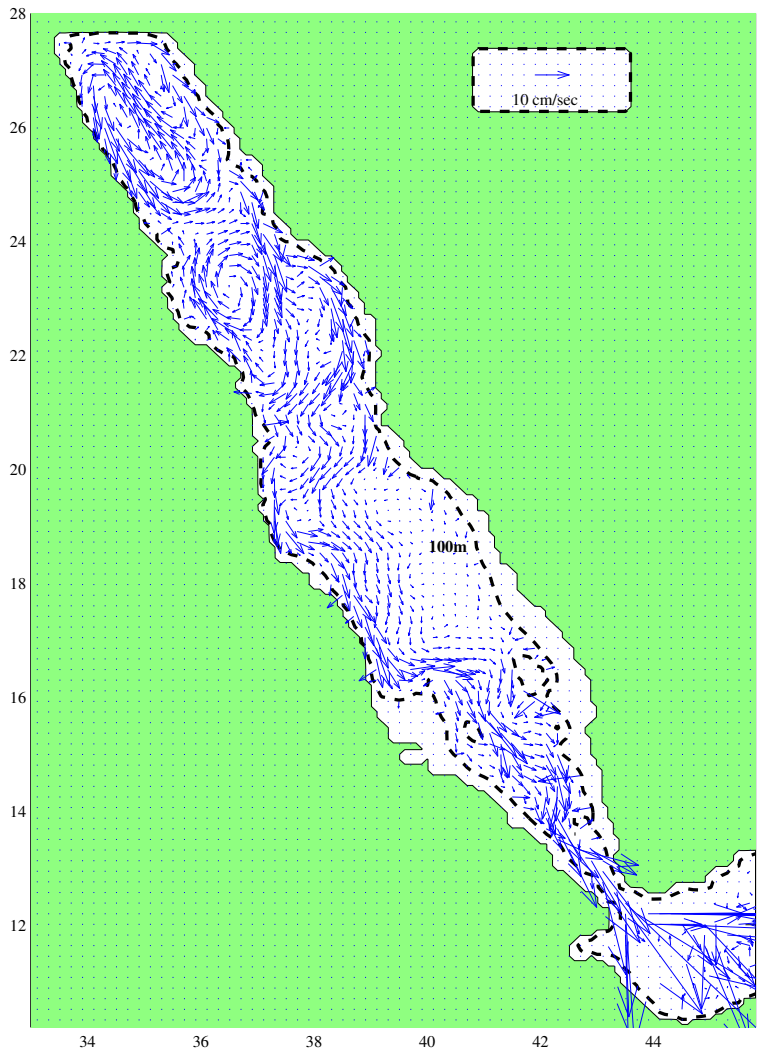
10 cm/sec
100m
28
26
24
22
20
18
16
14
12
34
36
38
40
42
44

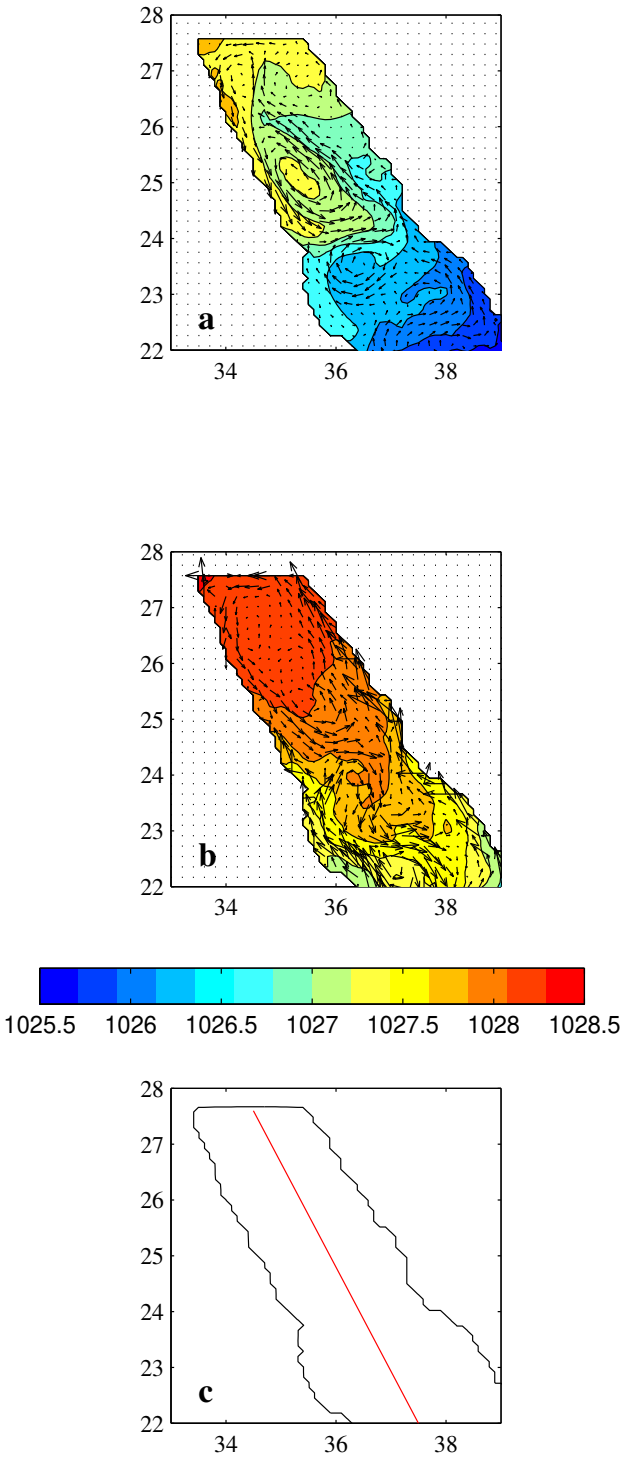
28
27
26
25
24
23
22
34
36
38
a
b
1025.5
1026
1026.5
1027
1027.5
1028
1028.5
c

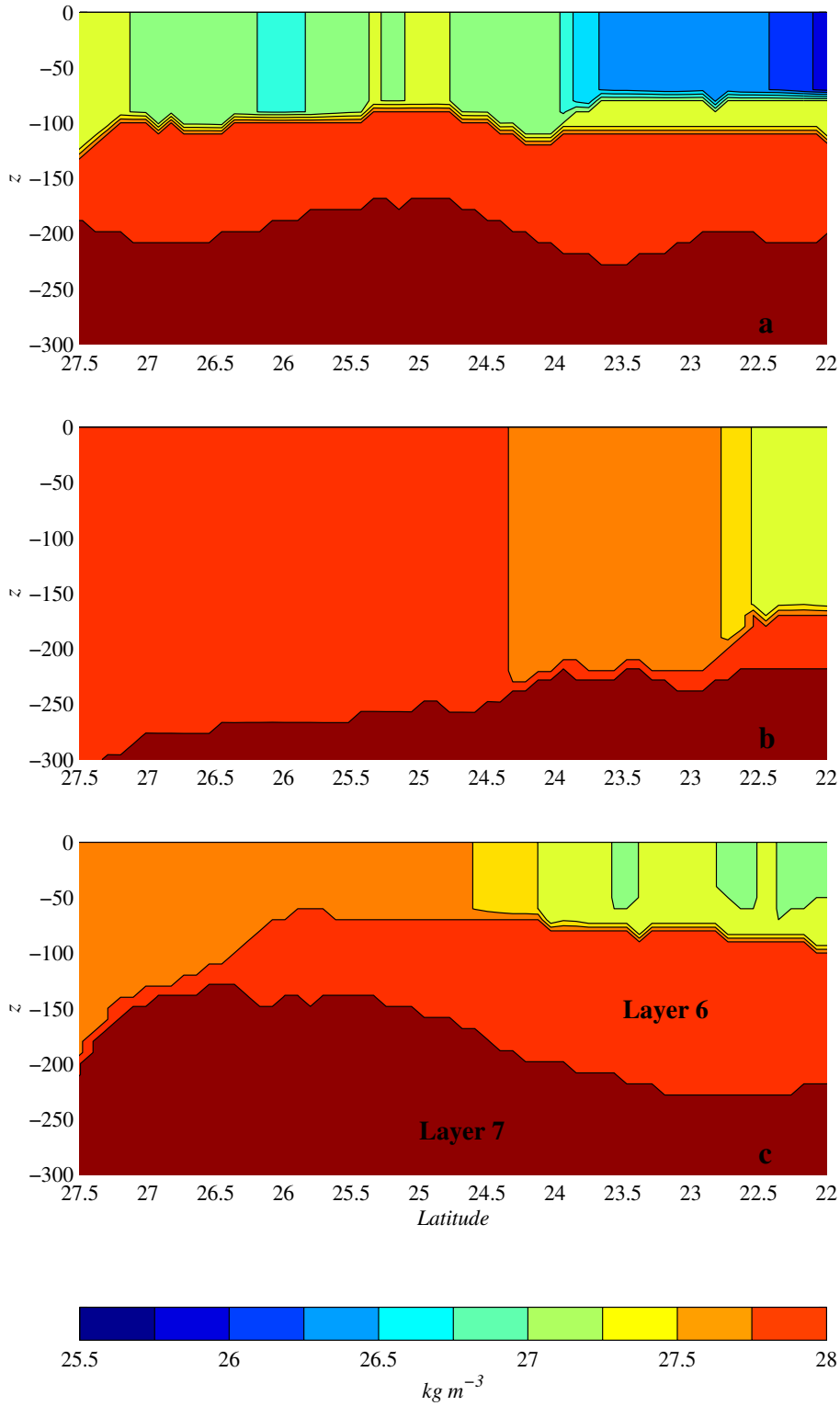
0
−50
−100
−150
−200
−250
−300
z
a
b
Layer 6
Layer 7
c
27.5
27
26.5
26
25.5
25
24.5
24
23.5
23
22.5
22
Latitude
25.5
26
26.5
27
27.5
28
kg m−3

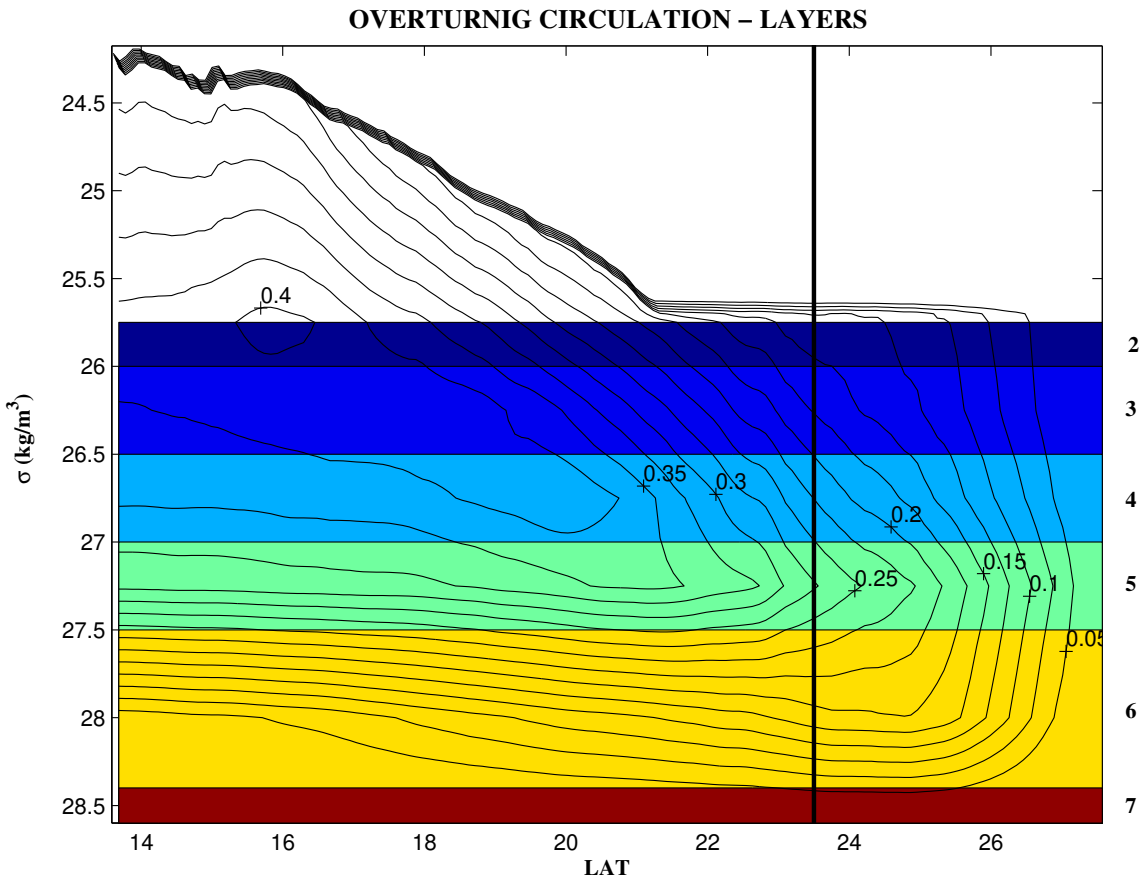
OVERTURNIG CIRCULATION – LAYERS
σ (kg/m3)
24.5
25
25.5
26
26.5
27
27.5
28
28.5
14
16
18
20
22
24
26
LAT
0.4
0.35
0.3
0.2
0.25
0.15
0.1
0.05
2
3
4
5
6
7

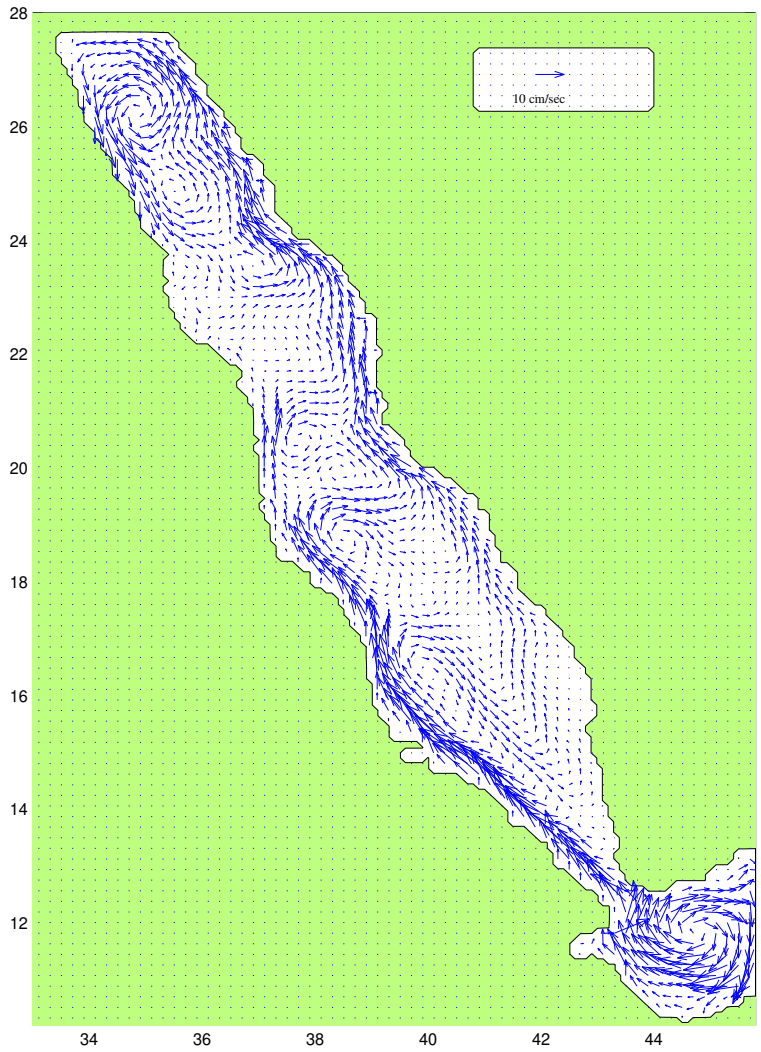
10 cm/sec
28
26
24
22
20
18
16
14
12
34
36
38
40
42
44

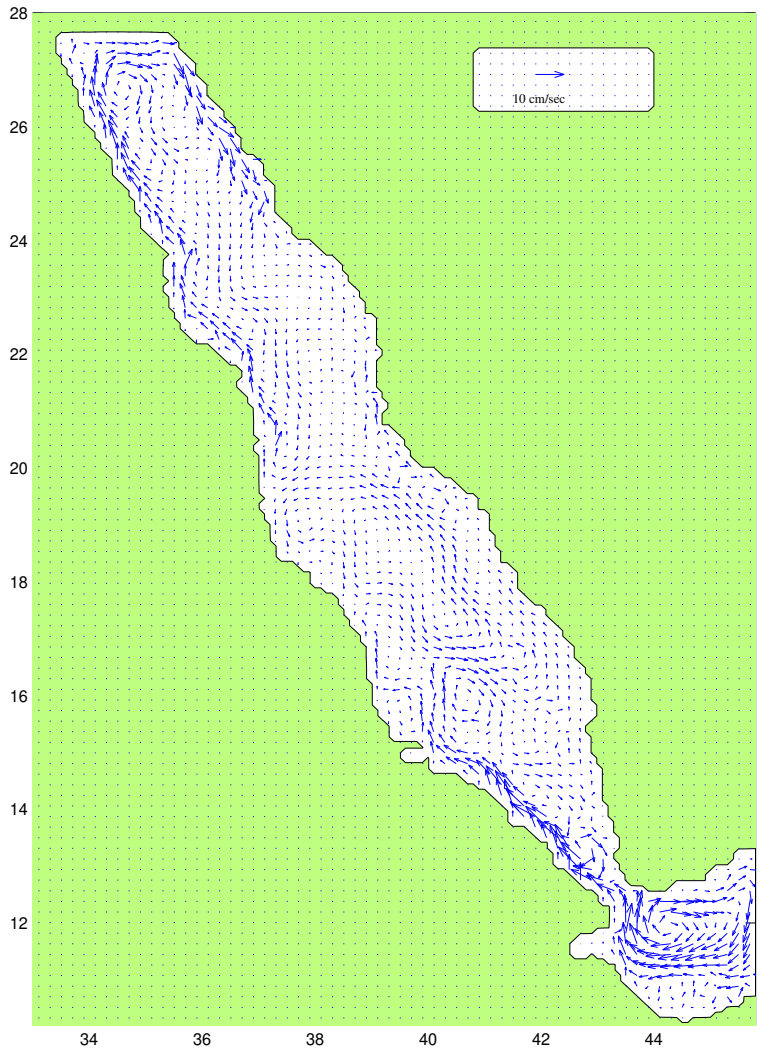
10 cm/sec
28
26
24
22
20
18
16
14
12
34
36
38
40
42
44

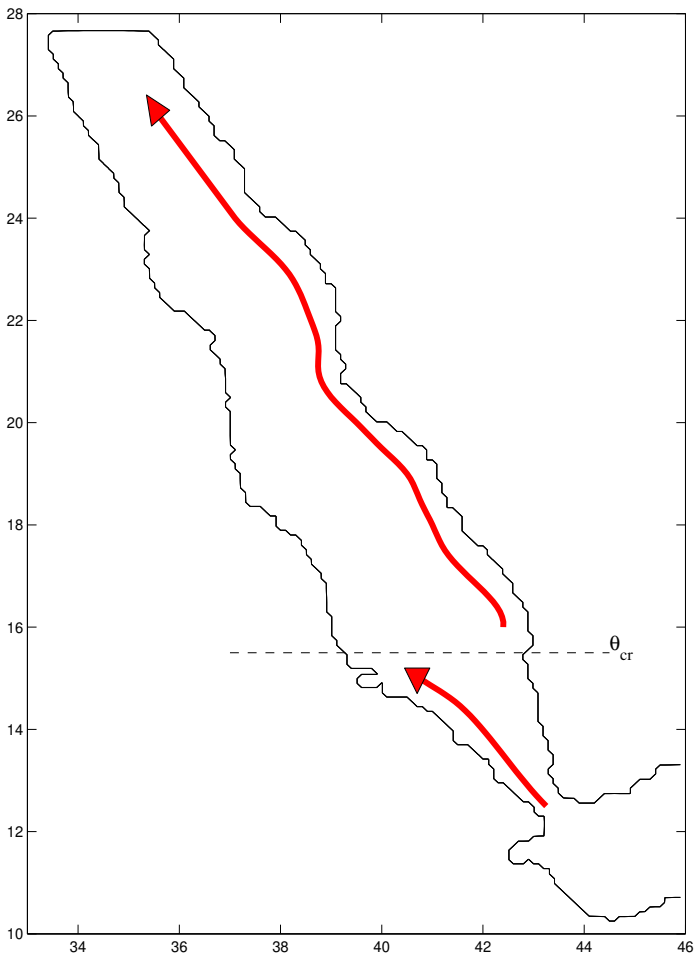
28
26
24
22
20
18
16
14
12
10
34
36
38
40
42
44
46
θcr